Available online at www.sciencedirect.com
ScienceDirect
International Journal of Heat and Mass Transfer 50 (2007) 2078–2088
International Journal of HEAT and MASS TRANSFER
www.elsevier.com/locate/ijhmt

Two-phase flow instability for boiling in a microchannel heat sink

K.H. Chang, Chin Pan *

Department of Engineering and System Science, National Tsing Hua University, Hsinchu 30043, Taiwan, ROC

Received 27 June 2006; received in revised form 10 November 2006
Available online 18 January 2007

Abstract

The present study explores experimentally the two-phase flow instability in a microchannel heat sink with 15 parallel microchannels. The hydraulic diameter for each channel is 86.3 μm. Flow boiling in the present microchannel heat sink demonstrates significantly different two-phase flow patterns under stable or unstable conditions. For the stable cases bubble nucleation, slug flow and slug or annular flows appear sequentially in the flow direction. On the other hand, forward or reversed slug/annular flows appear alternatively in every channel. Moreover, the length of bubble slug may oscillate for unstable cases with reversed flow demonstrating the suppressing effect of pressure field for bubble growth. It is found that the magnitude of pressure drop oscillations may be used as an index for the appearance of reversed flow. A stability map on the plane of inlet subcooling number versus phase change number is established. A very narrow region for stable two-phase flow or mild two-phase flow oscillations is present near the line of zero exit quality.

Keywords: Microchannel; Flow boiling; Two-phase flow; Two-phase flow instability

1. Introduction

Microchannel heat sinks have been proposed for the cooling of microelectronics because of their potentially high heat transfer capability. Recently, there have been abundant literatures on the study of boiling heat transfer in mini- or microchannels. For example, Lin et al. [1], Chen et al. [2], Qu and Mudawar [3], Lee et al. [4,5], Li et al. [6], Thome et al. [7], Zhang et al. [8] and Kandlikar [9] investigated flow boiling in mini- or microchannels. In particular, flow instability, which is of significant concern for the design of a two-phase flow system, has been reported in several previous studies on minichannels or microchannels, especially in parallel systems. Kennedy et al. [10] explored the onset of flow instability in uniformly heated horizontal microchannels. Kandlikar [11] reported flow instability in electrically heated multi-minichannel evaporators consisting of six parallel minichannels with visual confirmation of complete flow reversal in some of the channels. Li et al. [12,13] reported two-phase flow instability of flow boiling in two parallel triangular and trapezoidal microchannels, respectively, with a hydraulic diameter around 50 μm for both channels. The temporal evolution of temperatures at inlet and outlet chambers, the inlet pressure as well as the pressure drop from the inlet to outlet chamber during the experiments were recorded and analyzed with flow visualization. The results of their study demonstrated clearly two-phase flow instabilities with significant oscillations in two-phase flow properties at high heating powers and low mass flow rates. Flow visualization confirmed the presence of flow reversal during large amplitude oscillations. In particular, large magnitude, aperiodic oscillations appear with alternative presence of two-phase flow and single-phase vapor flow at high heat fluxes [13]. Wu and Cheng [14] reported three modes of two phase flow instability in multi-parallel microchannels having a hydraulic diameter of 186 μm. Qu and Mudawar [3] investigated hydrodynamic instability and pressure drop in a water-cooled two-phase microchannel heat sink containing 21 parallel 231 × 173 μm microchannels. They identified two types of two-phase flow instability, namely severe pressure

* Corresponding author. Tel.: +886 3 5725363; fax: +886 3 5720724.
E-mail address: cpan@ess.nthu.edu.tw (C. Pan).

0017-9310/$ - see front matter © 2006 Elsevier Ltd. All rights reserved.
doi:10.1016/j.ijheatmasstransfer.2006.11.014

Nomenclature

DP_{max}	the maximum instant pressure drop (kPa)
DP_{min}	minimum instant pressure drop (kPa)
G	mass flux (kg/m^2 s)
i_{in}	the liquid enthalpy at the channel inlet (J/kg)
i_ℓ	the enthalpy of saturated liquid at the system pressure (J/kg)
$i_{\ell v}$	the latent heat of evaporation at the system pressure (J/kg)
i_{sub}	$i_\ell - i_{in}$ (J/kg)
i_v	the enthalpy of saturated vapor at the system pressure (J/kg)
$L(t)$	instant bubble length in slug flow at time t (μm)
$L(t_0)$	bubble length in slug flow at the reference time, t_0 (μm)
Lr	bubble length ratio, $L(t)/L(t_0)$
N_{pch}	subcooling number, $\left(\frac{Q_c \upsilon_{lv}}{W i_{lv} \upsilon_l}\right)$
N_{sub}	phase change number, $\left(\frac{i_{sub} \upsilon_{lv}}{i_{lv} \upsilon_l}\right)$
q''	heat flux (kW/m^2)
Q_c	the heat transfer rate to the channel (J/s)
t	time (s)
t_0, t_1, t_2	reference time (s)
υ_l	the specific volume of saturated liquid at the system pressure (m^3/kg)
υ_{lv}	the specific volume difference between vapor and liquid at the system pressure (m^3/kg)
v_v	the specific volume of saturated vapor at the system pressure (m^3/kg)
W	the total mass flow rate to the channels (kg/s)
x_e	the exit vapor quality

Greek symbol

β	coefficient of exponent for bubble growth in slug flow (s^{-1})

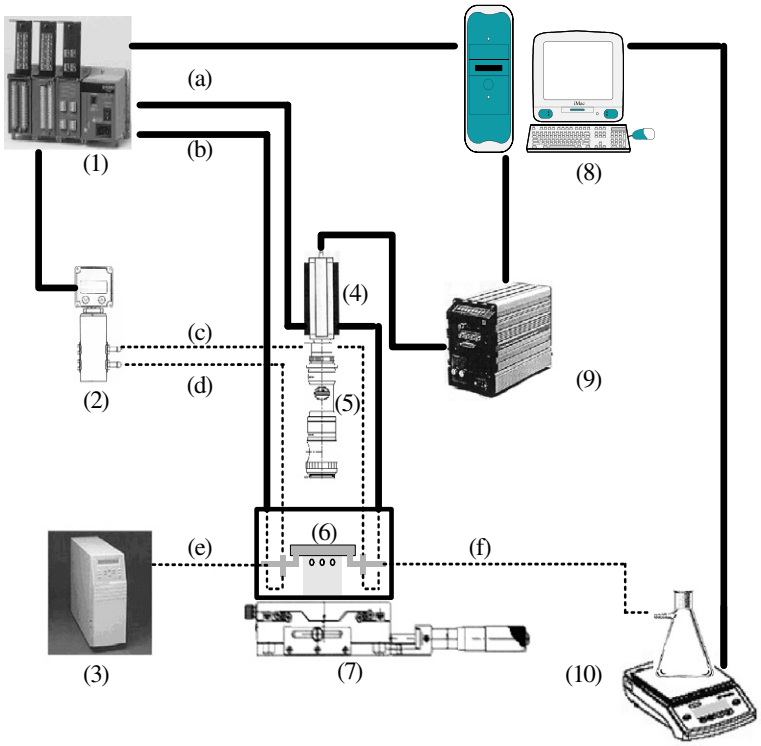

(1) Data Acquisition System
(2) Differential pressure transmitter
(3) HPLC pump
(4) CCD
(5) Micro-lens
(6) Microchannel (text section)
(7) x-y stage
(8) Computer
(9) CCD processor
(10) Electronic balance
(a) Inlet temperature
(b) Outlet temperature
(c) Outlet pressure
(d) Intlet pressure
(e) Pure water inlet
(f) Pure water outlet

(a)

Fig. 1. (a) The experimental setup. (b)-1 Top view of the test section. (b)-2 Cross-section view of A–A′ section and locations of thermocouples. (b)-3 Cross-section view of B–B′ section.

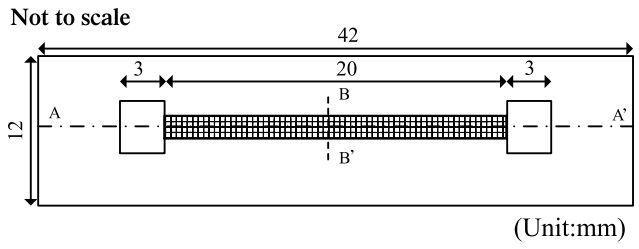

(b)-1

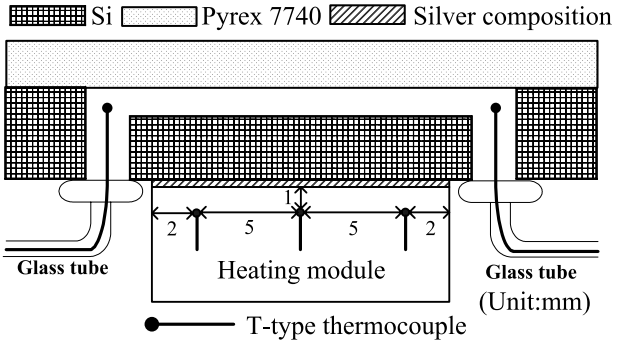

(b)-2

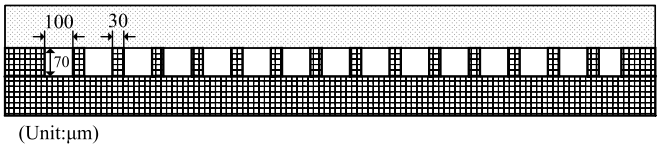

(b)-3

Fig. 1 (*continued*)

drop oscillations and mild parallel channel instability. Hetsroni et al. [15] studied experimentally instability and heat transfer phenomenon under condition of periodic flow boiling in parallel triangular microchannels. In-phase oscillations of pressure drop, fluid temperature at the outlet manifold, and mean and maximum heater temperature were reported. At a constant value of mass flux, the oscillation amplitude was found to increase with increase in heat flux.

Two-phase flow instability in a multi-channel system is different from that in a single-channel system due to very complicated channel-to-channel interactions [16]. In parallel microchannel systems, such interactions could be more complicated than that in ordinarily sized channels. This is because that the dividing wall between two neighboring channels must be very thin and the two channels could interact with each other through the conduction of dividing wall in addition to their common inlet and outlet. The present work investigates experimentally two-phase flow instability for flow boiling in silicon-based, fifteen parallel rectangular microchannels with hydraulic diameter of 86.3 μm for each channel. The width and depth of each channel are 99.4 and 76.3 μm, respectively. The microchannels employed for the present work were prepared by silicon bulk micro machining and anodic bonding processes. The two-phase flow patterns under boiling conditions were visualized using a high-speed digital CCD camera and analyzed with the measurement of temperatures at the heating surface, the inlet and outlet chambers, and the pressure drop from inlet to outlet chamber to understand the instability behavior.

2. Experimental details

2.1. Experimental setup

Fig. 1a illustrates the experimental setup, consisting of a high pressure liquid chromatography (HPLC) pump, the test section with parallel microchannels and inlet/outlet chambers, a heating module and a flow visualization system. Fig. 1b illustrates the details of the test section including the geometry of each channel, dividing island, and inlet/outlet chambers. The locations of thermocouples inside the inlet/outlet chambers and embedded in the heating module are also shown in Fig. 1b-2. The cross-section view from a SEM of a test section with 10 parallel

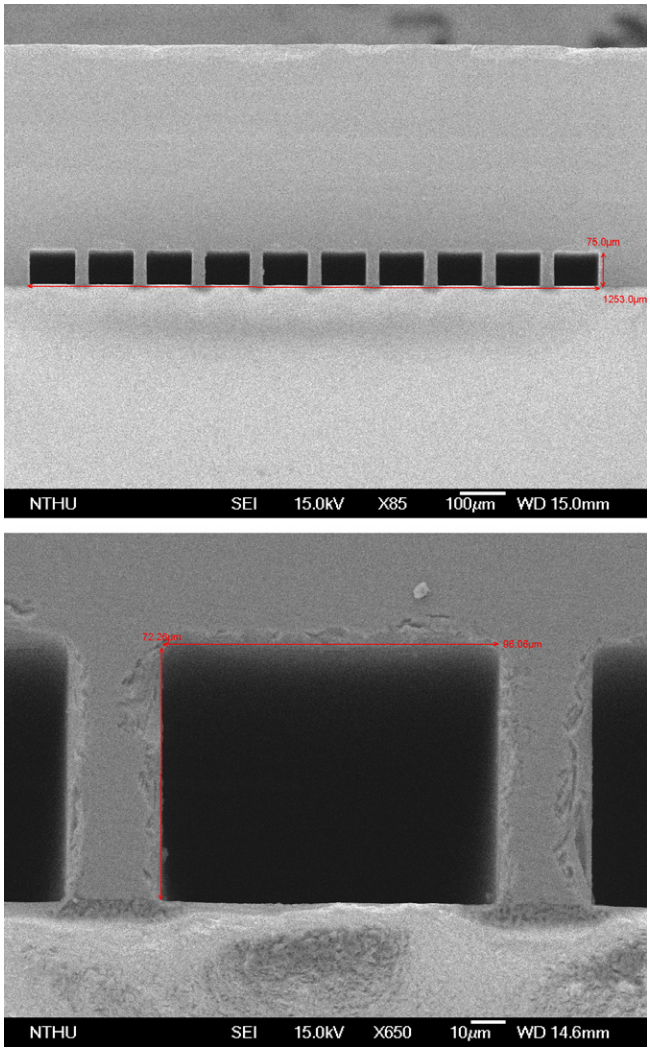

Fig. 2. SEM images showing the parallel microchannels with rectangular cross-section.

microchannels is exhibited in Fig. 2. The test section with the silicon-based microchannels was adhered with silver composition (DuPont Electronic, 4817 N) on top of the heating module, which is a copper block heated by a heating element with controllable power. The top surface dimension of the heating module is 12 mm × 42 mm. Three T-type thermocouples were embedded 1 mm under the surface to measure the heating surface temperature. It was found that the temperature difference among these three locations is within one degree. The small temperature difference may result from the large thermal conductivity of copper. The temperature at the central location is reported here. The channel wall temperature can thus be obtained considering the thermal resistance from the location of thermocouple to the bottom wall of the channel [5]. The side surfaces of the heating module were insulated with plasters and heat resistance plate. Moreover, to minimize heat loss, the whole heating module and test section were covered with thick ceramic fiber except the upper portion of the test section to allow for flow visualization. The channel wall heat flux and heat loss through various paths can be determined by considering energy balance in the system [5].

The forced flow of de-ionized water in the microchannel was provided by a HPLC pump with a flow range from

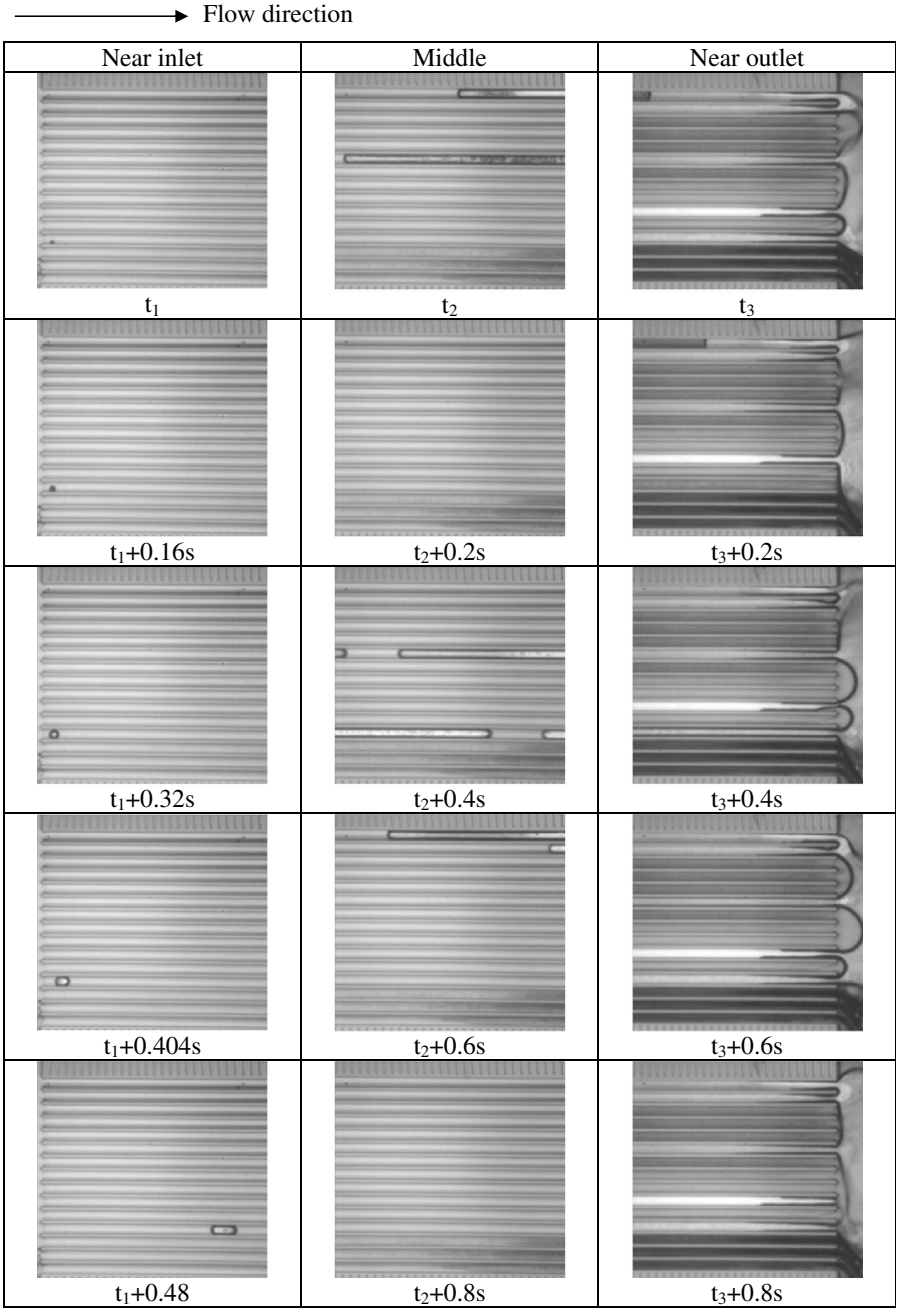

Fig. 3. Evolution of two-phase flow patterns in the entrance, middle and exit regions for a stable case, $G = 22\ \mathrm{kg/m^2\,s}$, $q'' = 7.91\ \mathrm{kW/m^2}$.

0.01 to 10.0 ml/min. A Whatman injector filter with a net size of 0.1 μm was added at the exit of the syringe pump to prevent sub-microparticles from entering the microchannels. An electronic balance, which provides an independent measurement of the flow rate, was placed at the exit to measure the two-phase flow mixture collected. However, only the mean flow rate was examined. It has been confirmed that the flow driven by the HPLC pump was quite steady based on the weight-time relationship from the electronic balance.

The flow visualization system includes a high-speed digital camera (KODAK motion coder SR-ultra), a monitor and a personal computer. To observe the two-phase flow pattern in the microchannel, a microlens was mounted on the CCD. The maximum frame rate available of the camera is 10,000 frame/s and the maximum shutter speed is 1/20,000. Typically the frame rate was set at 250 frame/s for the present study to have good resolution in the observation window. An x–y–z mechanism was installed with the test module to hold the lens and provide accurate position along the test plane (x–y-plane) and focusing (y-direction).

The temperatures at the inlet and outlet chambers were measured using T-type thermocouples. The pressure drop from inlet to outlet chamber, as shown in Fig. 1, was measured by a differential pressure transmitter. The output of the thermocouples and pressure transducers were recorded by a data acquisition system (YOKOKAWA MX100). The

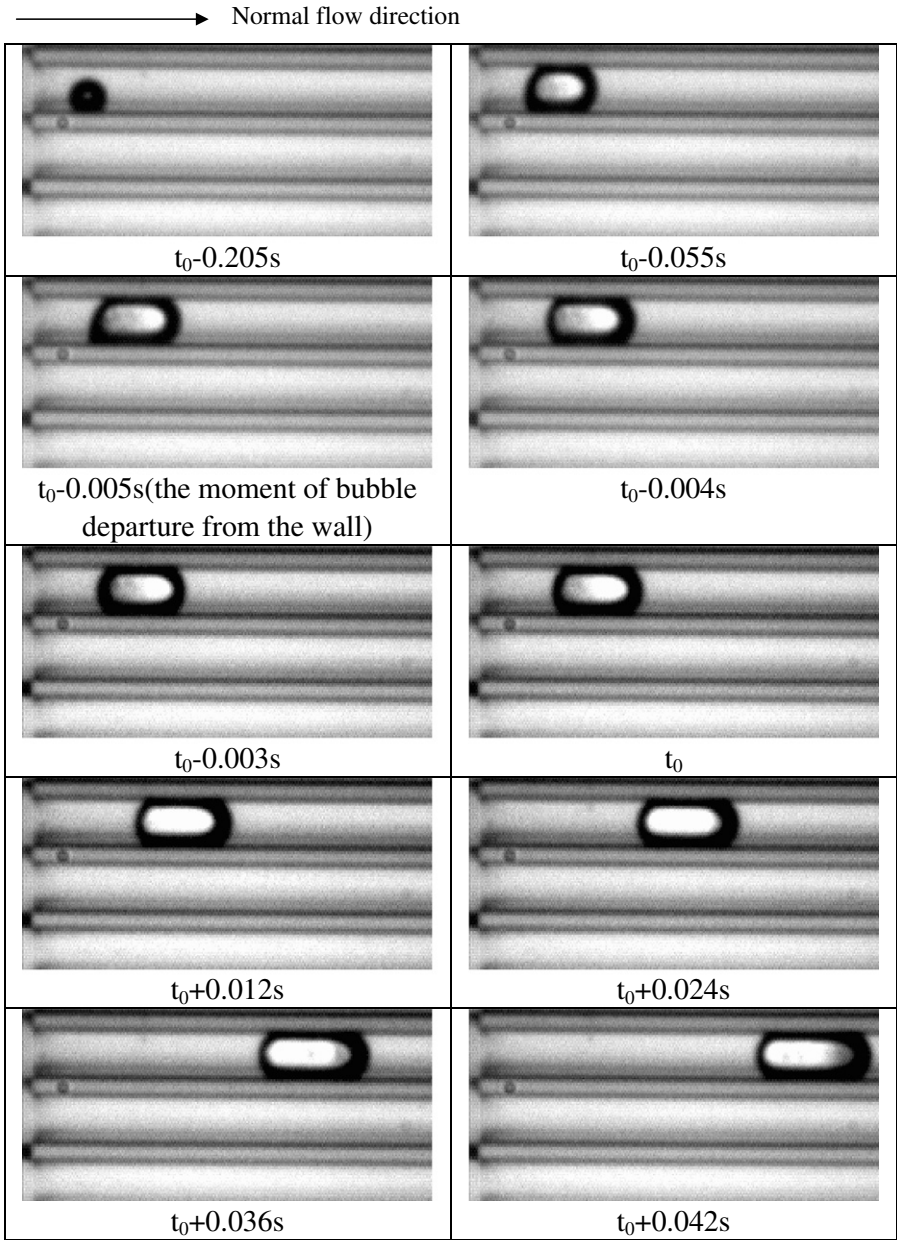

Fig. 4. Growth of bubble length for a stable case for $G = 22\ \mathrm{kg/m^2\,s}$, $q'' = 7.91\ \mathrm{kW/m^2}$ (the second cycle of Fig. 5).

measurement uncertainty for flow rate in the microchannels after calibration was estimated to be ±4%. The uncertainties in temperature measurements were ±0.2 °C for the T-type thermocouples. The measurement uncertainty of pressure transducer was 0.5%. The uncertainties in surface heat flux was estimated to be from ±1.88% to ±49.7% with an average uncertainty of 16.6%. The heat flux uncertainty generally decreases with increasing heat flux and/or mass flux.

3. Results and discussion

Fig. 3 illustrates the evolution of two-phase flow pattern in the microchannel array for $G = 22\ \mathrm{kg/m^2\,s}$ and $q'' = 7.91\ \mathrm{kW/m^2}$. This is the onset heat flux for nucleate boiling to occur. The two-phase flow for this case is considered to be stable. Moreover, this is the case with the highest heat transfer coefficient for this particular flow rate. For the inlet region, which is located right next to the inlet chamber, basically single phase flow prevails except one bubble is nucleating in one of the channels, i.e., the fourth channel from the bottom in the figure during the time interval of this observation. The bubble becomes a bubble slug 0.40 s after its nucleation. The length of the bubble slug will then exponentially grow through the evaporation of the microlayer between the bubble slug and channel wall as will be discussed further associated with Fig. 4. Long bubble slugs or possibly annular flow appear in the middle region, which is located at approximately the middle part of the channel. Such slug flow or annular flow prevails for the region right before the channel exit. Vapor, possibly with the liquid film, flows out from various different channels from time to time. It should be noted that the flow patterns at three different locations were not observed at the same time interval but began at three different reference times, t_1, t_2 and t_3, respectively.

Fig. 4 demonstrates, for the above stable case, the growth of slug bubble in the axial direction while it is moving in the flow direction. At 0.005 s before the reference time, the elongated bubble is at the moment of departure from the surface. At this and right after this moment, the bubble length is somewhat longer than that at the reference time due to the surface tension, which tends to keep the bubble on the wall and elongate the bubble by counteracting with drag of bulk flow. For some short time interval after detachment, the bubble restores a minimum length at the reference time. Li et al. [6] have demonstrated that the growth of the bubble slug in the microchannel is resulted from the balance between the bubble expansion due to evaporation of thin liquid film next to the heating wall and the suppression effect due to the pressure field around the bubble. Fig. 5 demonstrates that bubble length, indeed, grows exponentially, though not very smoothly possibly due to the variation of pressure field around the bubble. The numerical value for the coefficient of exponent is in the same order of magnitude as those reported by Li et al. [6].

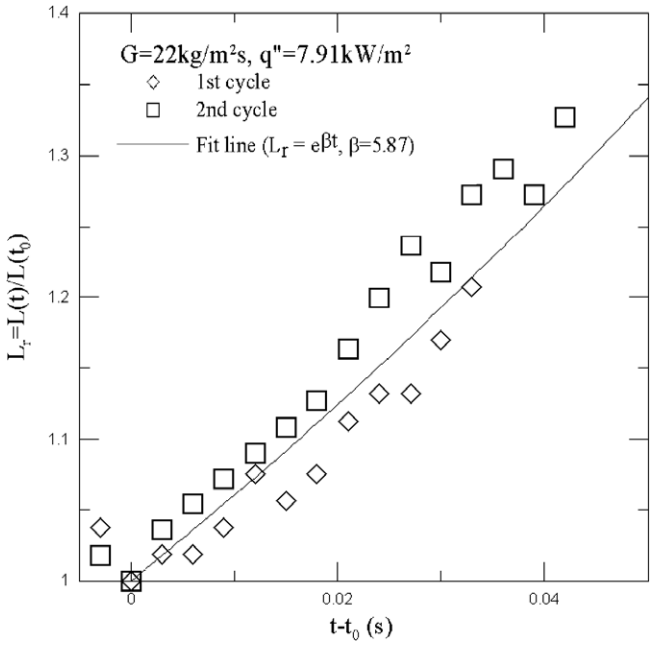

Fig. 5. The exponential growth of bubble length for $G = 22\ \mathrm{kg/m^2\,s}$, $q'' = 7.91\ \mathrm{kW/m^2}$.

Fig. 6 displays significantly different two-phase flow patterns in the microchannel array for $G = 22\ \mathrm{kg/m^2\,s}$ and $q'' = 15.8\ \mathrm{kW/m^2}$. The flow rate for this case is same as the previous case but the heat flux is about twice higher. The two-phase flow for this case is unstable. Forward and reversed slug or annular flows appear alternatively in every channel. Forward flow of two-phase mixture to the outlet chamber and reversed two-phase flow to the inlet chamber can be clearly observed frequently. Fig. 7 displays a similar unstable two-phase flow pattern for $G = 44\ \mathrm{kg/m^2\,s}$ and $q'' = 87.7\ \mathrm{kW/m^2}$. For this case, slug and annular flows appear in the near inlet region and reversed two-phase flow to the inlet chamber intermittently can be clearly visualized. Fig. 7 demonstrates reversed slug flow to the inlet chamber at t_1, $t_1 + 0.032$ s, and $t_1 + 0.048$ s. As for the middle region, slug and annular flows appear. The near exit region shows more frequent two-phase flow to the exit chamber. In fact, Fig. 7 demonstrates forward two-phase mixture to the outlet chamber in every frame.

Significant pressure drop oscillations appear under such unstable situations, as shown in Fig. 8 for the cases of $G = 44\ \mathrm{kg/m^2\,s}$ and $q'' = 78.6$ and $87.7\ \mathrm{kW/m^2}$, respectively. Such large-magnitude pressure drop oscillations may result in the length of bubble slugs growing and shrinking alternatively as demonstrated in Figs. 9 and 10 for $G = 44\ \mathrm{kg/m^2\,s}$ and $q'' = 87.7\ \mathrm{kW/m^2}$. As discussed earlier, the bubble growth may be limited by the pressure field around the bubble. Consequently, it is not surprised to see the oscillation of bubble length under such unstable situations with significant pressure oscillations. Such bubble length oscillation during unstable flow further supports the thin film evaporation model proposed by Li et al. [6].

Indeed, the magnitude of pressure drop oscillations may be employed as an index to distinguish whether or not an operation state is stable. Fig. 11 shows that if DP_{max}–DP_{min}, which is defined as the maximum instant pressure drop minus the minimum instant pressure drop, is smaller than 6 kPa, the system is either stable or of mild oscillations with small magnitude and without reversed flow to the inlet chamber. On the other hand, if it is greater than

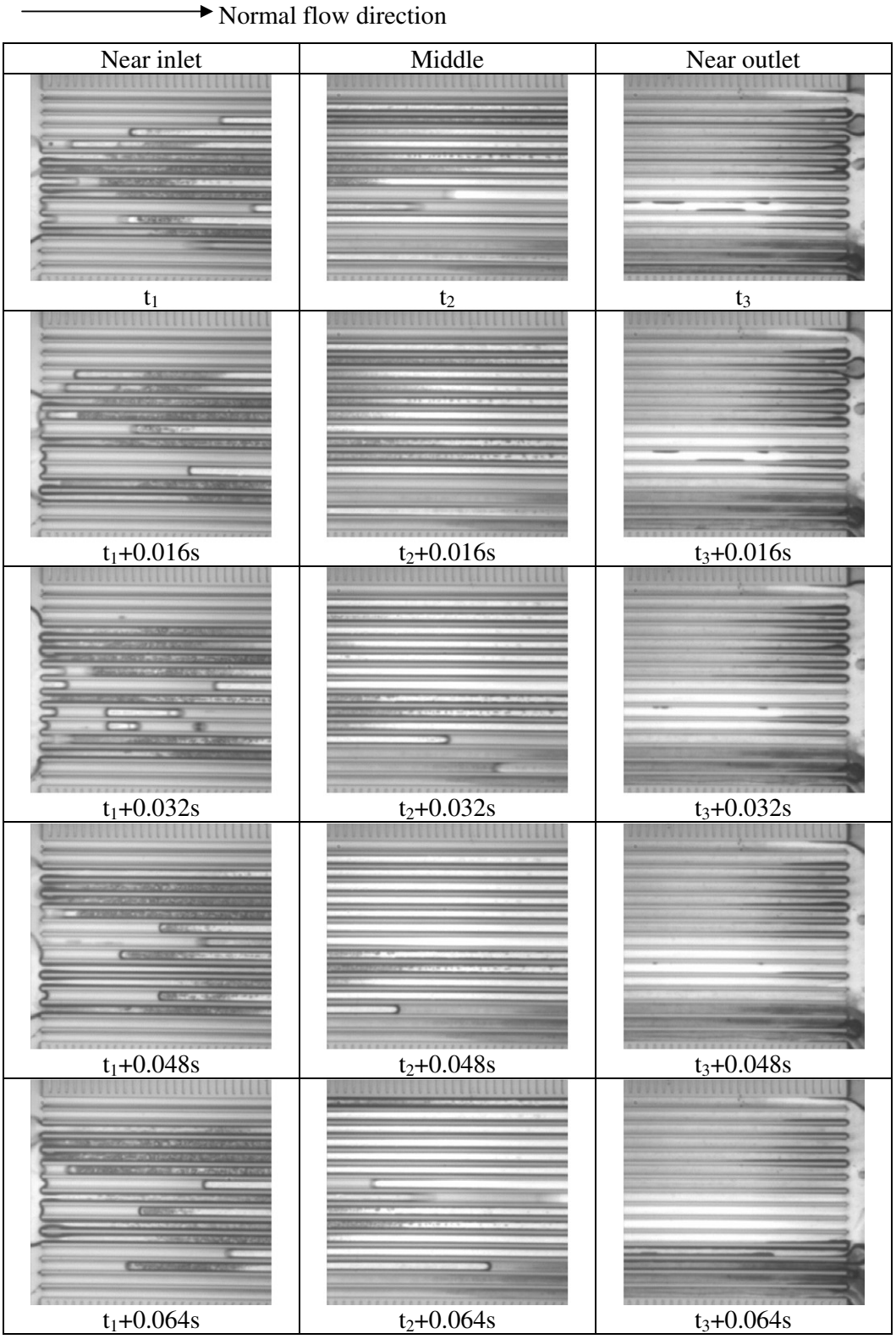

Fig. 6. Time evolution of two-phase flow patterns in the entrance, middle, and exit regions for an unstable case. ($G = 22$ kg/m^2 s, $q'' = 15.8$ kW/m^2).

6 kPa, reversed two-phase flow with large magnitude oscillations appears and the system is considered unstable.

Traditionally, the stability map of two-phase flow is presented on the plane of subcooling number (N_{sub}) versus phase change number (N_{pch}). These two non-dimensional numbers are defined as follows:

$$N_{sub} \equiv \frac{i_{sub}}{i_{lv}} \frac{\upsilon_{lv}}{\upsilon_l} \tag{1}$$

and

$$N_{pch} \equiv \frac{Q_c}{Wi_{lv}} \frac{\upsilon_{lv}}{\upsilon_l} \tag{2}$$

where i_{lv} is the latent heat of evaporation at the system pressure; $i_{sub} = i_l - i_{in}$ is the inlet subcooling; i_l is the enthalpy of saturated liquid at the system pressure; i_{in} is the liquid enthalpy at the channel inlet, i.e., inlet chamber; Q_c is the heat transfer rate to the channels; W is the total mass flow rate to the channels; υ_l is the specific volume of saturated liquid at the system pressure; υ_v is the specific volume of saturated vapor at the system pressure; $\upsilon_{lv} = \upsilon_l - \upsilon_v$. The inlet pressure is designated as the system pressure, at which thermo-physical properties, as indicated above, are evaluated. Eq. (1) indicates that the subcooling number is proportional to the inlet subcooling. For the present study,

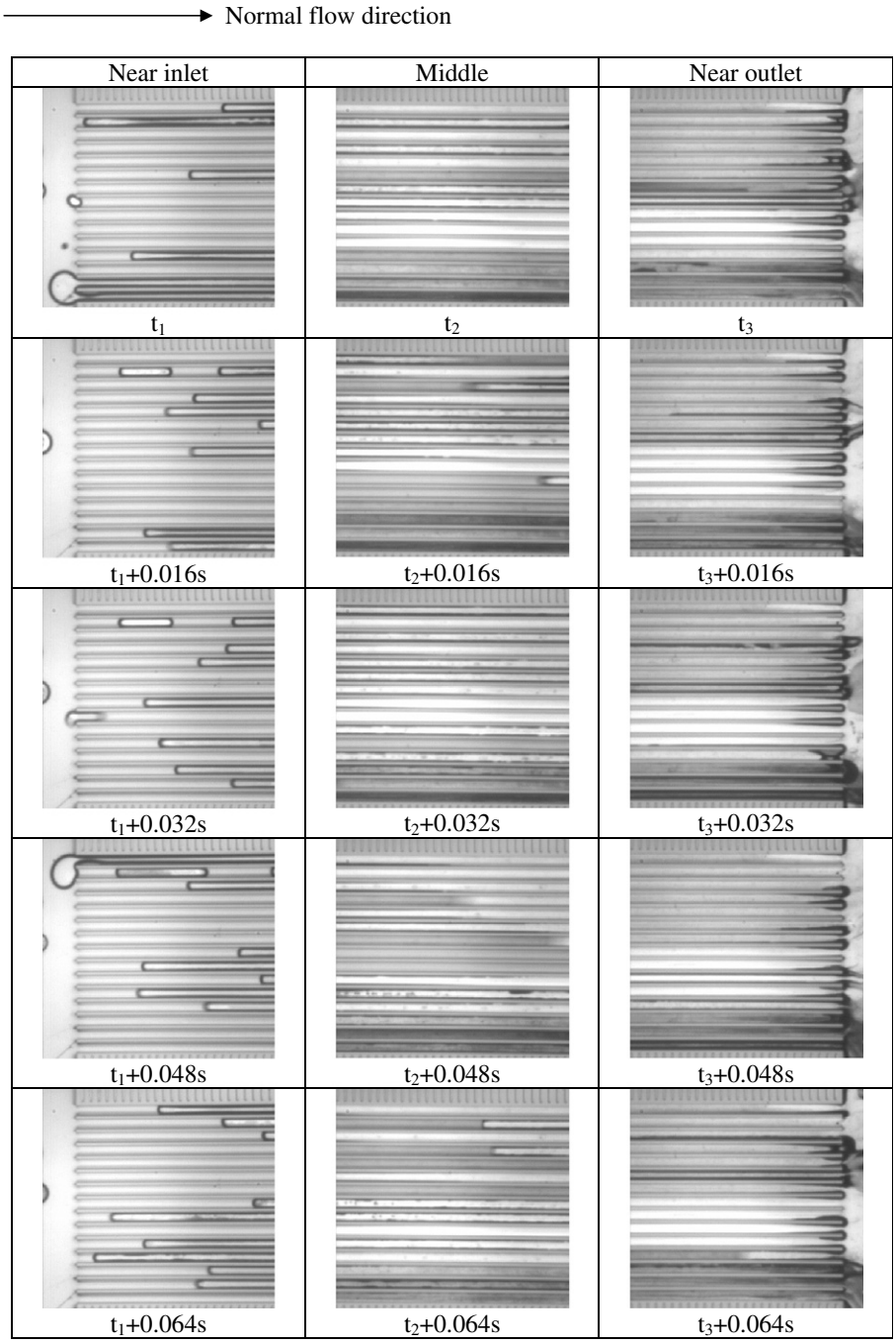

Fig. 7. Time evolution of two-phase flow patterns in the entrance, middle and exit regions for an unstable case. ($G = 44$ kg/m^2 s, $q'' = 87.7$ kW/m^2).

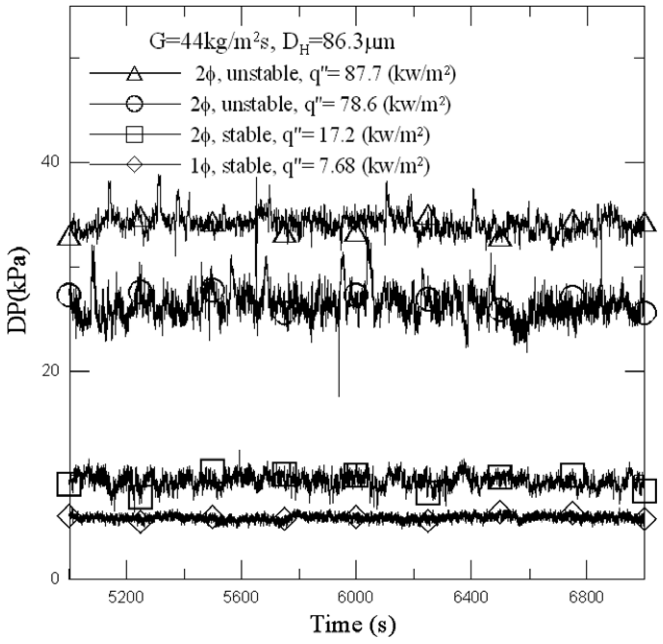

Fig. 8. Significant pressure drop oscillations under unstable conditions.

the inlet subcooling was not controlled as an independent variable but it was measured. It is found that it may vary with the heating power as well as the mass flow rate. On the other hand, the phase change number is proportional to the heating power to the channels and inversely proportional to the mass flux.

Fig. 12 illustrates the distribution of stable and unstable data on the plane of subcooling number versus phase change number mainly based on the results of the present study. Since the inlet subcooling is not a controlled variable, the data scatter significantly and more data are located in the region of high inlet subcooling, especially in the left side of $x_e = 0$, i.e., single-phase region, while the data in the region of low inlet subcooling is quite scarce. Nevertheless, a rough stability boundary can be obtained very close to $x_e = 0$. A very narrow region of stable two-phase flow or mild two-phase flow oscillations is present near the line of zero exit quality. The stability map shown in the figure is significantly different from that for an ordinarily sized boiling channel [17], which is an unstable region in the upper right part and otherwise stable on the plane of subcooling number versus phase change

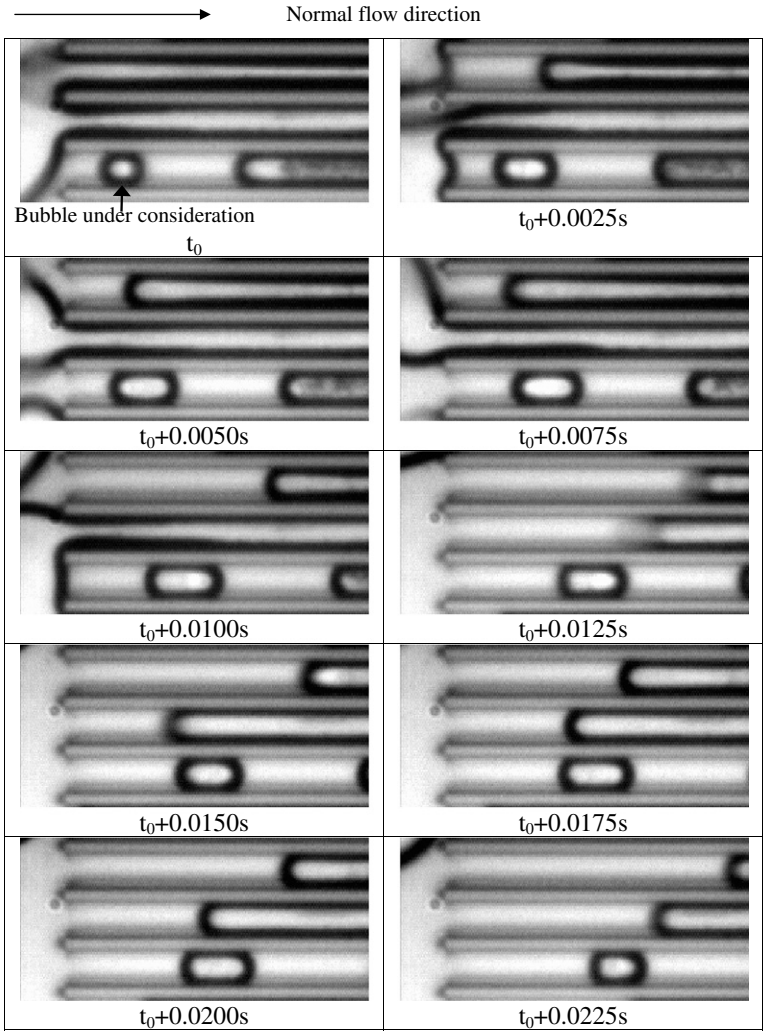

Fig. 9. Time evolution of bubble length for an unstable case, $G = 44\ \mathrm{kg/m^2\,s}$, $q'' = 87.7\ \mathrm{kW/m^2}$.

number. The data of Qu and Mudawar [18] are also displayed in Fig. 12 for comparison. They attributed the occurrence of the critical heat flux in the microchannel array to the appearance of significant two-phase flow instability with reversed flows. Although Qu and Mudawar tried to control their inlet subcooling, they commented that the inlet subcooling was lost during the event of the critical heat flux. The data shown are with their original inlet subcoolings. Even without true inlet subcooling, Fig. 12 shows

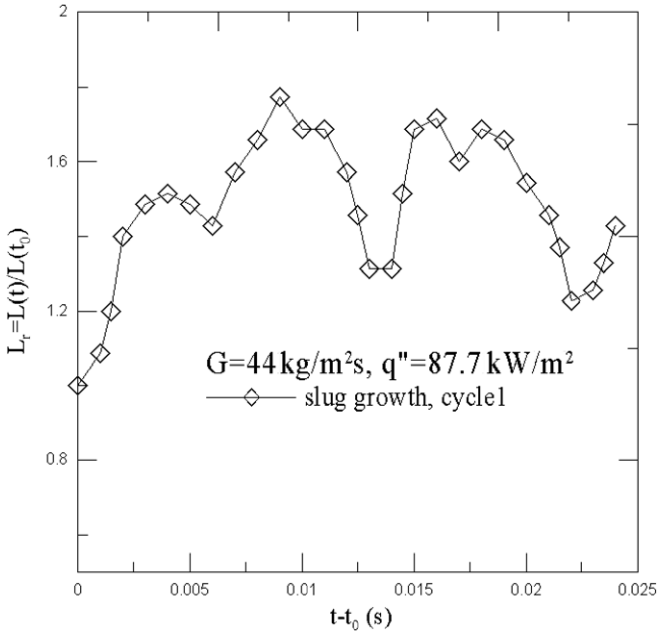

Fig. 10. Time evolution of bubble length ratio for an unstable case, $G = 44$ kg/m^2 s, $q'' = 87.7$ kW/m^2.

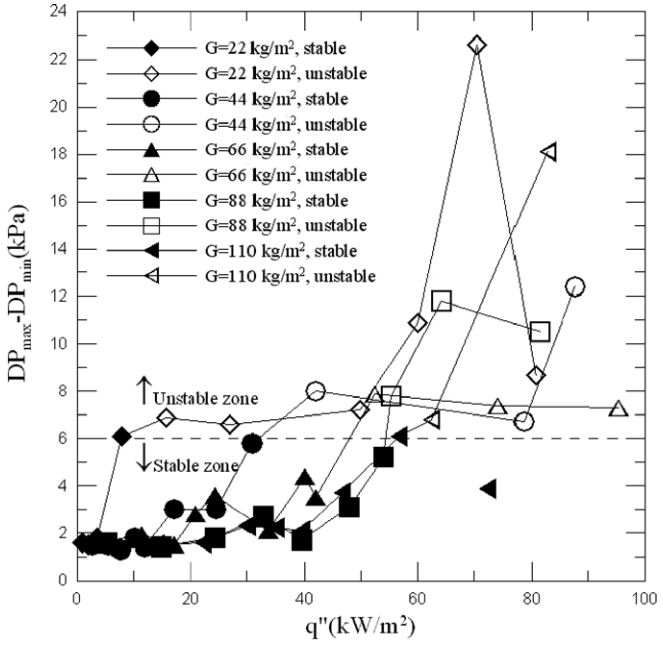

Fig. 11. Maximum magnitude of pressure drop oscillations for various cases.

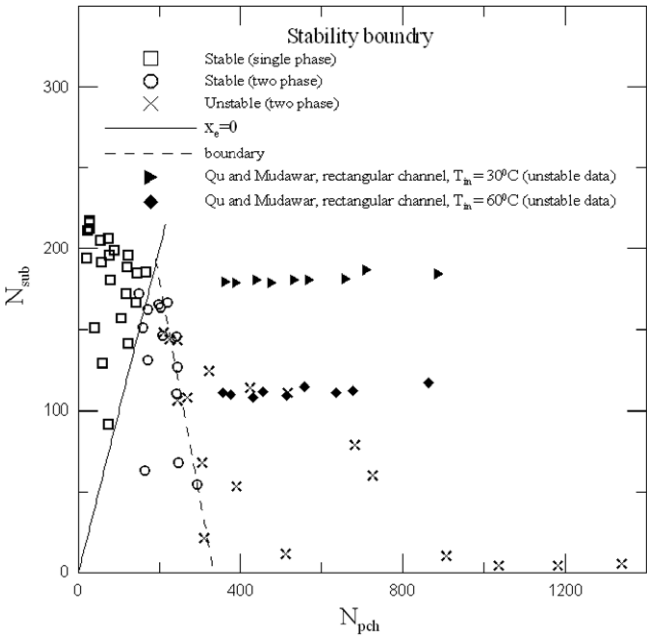

Fig. 12. Stability boundary on the plane of subcooling number versus phase change number.

that all of Qu and Mudawar's data are located within the unstable region of the present study. With the lost of inlet subcooling, both sets of their data should be lowered to the region with lower inlet subcooling.

4. Summary and conclusions

The present study investigated the two-phase flow instability in a microchannel heat sink with 15 parallel microchannels. The following conclusions may be drawn from the results of this work.

1. Flow boiling in the present microchannel heat sink demonstrates significantly different two-phase flow patterns under stable or unstable conditions. For the cases with stable two-phase flow or mild two-phase flow oscillation, bubble nucleation, slug flow and annular flow appear sequentially in the flow direction. On the other hand, for unstable cases forward or reversed slug or annular flows appear alternatively in every channel. Intermittently reversed flow of two-phase mixture to the inlet chamber can be clearly observed.
2. The length of bubble slug may grow exponentially for stable cases or oscillate for unstable cases with reversed flow indicating that the pressure field may suppress the bubble growth as suggested by Li et al. [6].
3. The magnitude of pressure drop oscillations may be used as an index for the appearance of reversed flow. The present study shows that if the deviation between the maximum instant pressure drop and the minimum instant pressure drop is greater than about 6 kPa, two-phase flow instability with reversed flow to the inlet chamber appears.

4. A traditional stability map on the plane of inlet subcooling number versus phase change number with a rough stability boundary is established. The stability boundary is significantly different from that for an ordinarily sized boiling channel. A very narrow region of stable two-phase flow or mild two-phase flow instability is present near the line of zero exit quality.

Acknowledgements

This work was supported by the National Science Council of Taiwan, ROC, under the contract NSC 92-2212-E-007-037. Figs. 3, 4, 6, 7 and 9 were prepared by Mr. P.C. Lee from the original video files. Figs. 5, 8, 10, 11 and 12 were also re-examined and re-plotted by Mr. Lee. His excellent works are highly appreciated.

References

[1] S. Lin, P.A. Kew, K. Cornwell, Two-phase heat transfer to a refrigerant in a 1 mn diameter tube, Int. J. Multiphase Flow 22 (2001) 703–712.
[2] W.L. Chen, F.G. Tseng, C. Pan, Boiling heat transfer and pressure drop in silicon-based micro-channels, in: Proc. of pacific Rim Workshop on Transducers and Micro/Nano Technologies, Xiaman, China, July 22–24, 2002, pp. 307–310.
[3] W. Qu, I. Mudawar, Measurement and prediction of pressure drop in two-phase microchannel heat sinks, Int. J. Heat Mass Transfer 46 (2003) 2737–2753.
[4] P.C. Lee, H.Y. Li, C. Pan, Nucleate boiling heat transfer in silicon-based boiling channel, Paper 2003-47220, ASME Summer Heat Transfer Conference, Las Vegas, July 20–23, 2003.
[5] P.C. Lee, F.G. Tseng, C. Pan, Bubble dynamics in microchannels, (I) single microchannel, Int. J. Heat Mass Transfer 47 (2004) 5575–5589.
[6] H.Y. Li, F.G. Tseng, C. Pan, Bubble dynamics in microchannels (II) two parallel microchannels, Int. J. Heat Mass Transfer 47 (2004) 5591–5601.
[7] J.R. Thome, V. Dupont, A.M. Jacobi, Heat transfer model for evaporation in microchannels. Part I: presentation of the model, Int. J. Heat Mass Transfer 47 (2004) 3375–3385.
[8] L. Zhang, E.N. Wang, K.E. Goodson, T.W. Kenny, Phase change phenomena in silicon microchannels, Int. J. Heat Mass Transfer 48 (2005) 1572–1582.
[9] S.G. Kandlikar, Heat transfer mechanisms during flow boiling in microchannels, ASME J. Heat Transfer 126 (2004) 8–16.
[10] J.E. Kennedy, G.M. Roach Jr., M.F. Dowling, S.I. Addel-khalik, S.M. Ghiaasiaan, S.M. Jeter, Z.H. Quereshi, The onset of flow instability in uniformly heated horizontal microchannels, ASME J. Heat Transfer 200 (2000) 118–125.
[11] S.G. Kandlikar, Fundamental issues related to flow boiling in minichannels and microchannels, Exp. Therm. Fluid Sci. 26 (2002) 389–407.
[12] H.Y. Li, P.C. Lee, F.G. Tseng, C. Pan, Two-phase flow instability of boiling in a double microchannel system at high heating powers, in: Proc. 1st Int. Conf. On Microchannels and Minichannels, ICMM2003-1077, Rochester, New York, April 24–25, 2003, pp. 615–621.
[13] H.Y. Li, P.C. Lee, C. Pan, Two-phase flow instability of boiling in two parallel microchannels, J. Chin. Soc. Mech. Eng. 26 (2005) 27–34.
[14] H.Y. Wu, P. Cheng, Two large-amplitude/long-period oscillating boiling modes in silicon microchannels, in: Proc. 1st Int. Conf. on Microchannels and Minichannels, ICMM2003-1079, Rochester, New York, April 24–25, 2003, pp. 629–633.
[15] G. Hetsroni, A. Mosyak, E. Pogrebnyak, Z. Segal, Periodic boiling in parallel microchannels at low vapor quality, Int. J. Multiphase Flow 32 (2006) 1141–1159.
[16] J.D. Lee, C. Pan, Dynamics of multiple parallel boiling channel systems with forced flows, Nucl. Eng. Des. 192 (1999) 31–44.
[17] P. Saha, M. Ishii, N. Zuber, An experimental investigation of thermally induced flow oscillations in two-phase systems, J. Heat Transfer 98 (1976) 616–622.
[18] W. Qu, I. Mudawar, Measurement and correlation of critical heat flux in two-phase microchannel heat sinks, Int J. Heat Mass Transfer 47 (2004) 2045–2059.